ISSN (Print) 1226-1750
ISSN (Online) 2233-6656
Journal of Magnetics 22(3), 406-413 (2017) https://doi.org/10.4283/JMAG.2017.22.3.406

Magnetic and Dielectric Properties of $CoFe_2O_4$ and $Co_xZn_{1-x}Fe_2O_4$ Nanoparticles Synthesized Using Sol-Gel Method

Sewench N. Rafeeq[1], Mukhils M. Ismail[1]*, and Jameel M. A. Sulaiman[1,2]

[1]*Department of Applied Science, University of Technology – Baghdad, Iraq*
[2]*College of Dentistry – University of Mosul – Mosul – Iraq*

(Received 16 March 2017, Received in final form 24 April 2017, Accepted 25 April 2017)

Cobalt ferrite nanoparticles ($CoFe_2O_4$) and cobalt zinc ferrites with general formula $Co_xZn_{1-x}Fe_2O_4$ (x = 0.5, 0.6, 0.7) were prepared by sol-gel method at a low temperature with a final pH value of 7. Synthesized spinel ferrites were sintered at various temperatures (220, 400, 600, 800 and 1000°C). X-ray diffraction (XRD) was used to characterize the sizes of particles and structural properties. The average crystalline size of the prepared ferrite was ranged between 18-49 nm. The FTIR spectra however showed two strong absorption bands ranged between (1037.45-399.26 cm^{-1}), which is a spinel ferrite. The study also focused on several dielectric properties of the samples such as dielectric constant (ε'), dielectric loss tangent (tan δ) and complex dielectric constant (ε''). The variation of dielectric parameters (ε) and tanδ with frequency revealed that the dispersion was due to Maxwell-Wagner. Magnetization measurements showed that the coactivity (H_c), saturation magnetization (M_s), remanent magnetization (M_r) and squarenessremnance ratio ($R = M_r/M_s$) strongly depend on content of zinc.

Keywords : Sol-gel synthesis, Co-Zn ferrites, dielectric, magnetic properties

1. Introduction

Ferrite materials have been widely used through several studies on various materials for instance Cobalt-Zinc ferrite [1]. The magnetic properties of Zn-substituted Co-ferrites have attracted great consideration due to the importance of these materials for data storage application [1].

$CoFe_2O_4$ has inverse spinel structure with Co^{2+} ions in octahedral sites and Fe^{3+} ions are equally distributed between tetrahedral and octahedral sites, whereas $ZnFe_2O_4$ has usually normal spinel structure with Zn^{2+} ions in tetrahedral and Fe^{3+}in octahedral sites [2]. Ferrites are typically manipulated by auto catalytic decomposition [3], hydrothermal process [4-6], reverse micelles method [7], co-precipitation [8], microwave combustion method [9] and sol-gel route [10]. Sol-gel is regarded as an excellent technique to enhance the control over homogeneity, elemental composition and powder morphology [11]. In addition, uniform nanosized metal clusters can be achieved crucially to support the electrical and magnetic properties of the nanoparticles. These advantages serve the sol-gel route over the other traditional preparation methods of ceramic oxide composites [12].

The properties of the ferrites are vastly sensitive to the ferrite compositions and synthesis techniques. Waje *et al.* [13] prepared $Co_{0.5}Zn_{0.5}Fe_2O_4$ via applying mechanical alloying and sintering methods; dielectric studies of their specimen showed that permittivity remains constant with frequency and varies with the sintering temperature. Lopez *et al.* [14] recently synthesized Zn doped $CoFe_2O_4$ magnetic nanoparticles by using a co-precipitation method. They observed decrease in coercive field and particle size with the increase of Zn concentration. Hassadee *et al.* [15] reported decrease in the magnetization and the coercivity of Co-Zn ferrite with increasing zinc substance due to the magnetic behavior and the anisotropic nature of cobalt.

Gul *et al.* [16] investigated magnetic and electrical properties of $Co_{1-x}Zn_xFe_2O_4$ varying x from (0.0 to 0.6). A decrease in Neel's temperature with an increase in Zinc doping concentration was observed. Temperature dependent (dc) resistivity measurements indicated semiconductor nature of Co-Zn ferrites. Veverka *et al.* [17] studied

©The Korean Magnetics Society. All rights reserved.
*Corresponding author: Tel: +9647707347508
e-mail: mmismail009@gmail.com

© 2017 Journal of Magnetics

$Co_{1-x}Zn_xFe_2O_4$ around x = 0.6 because of potential applications of the composition in the magnetic fluid hyperthermia. It is reported that the cationic distribution in ferrite is more complex and the distribution is random in its nature. Veverka *et al.* [17] also observed that presence of vacancies in the octahedral sites change the cobalt ions partially or completely to the Co^{3+} state. A neutron diffraction study showed the differences of cationic distributions in nanoparticles and bulk ferrite samples.

Hence, the present work deals with sol-gel method synthesis nanoparticles of cobalt ferrite with formula $CoFe_2O_4$ and cobalt zinc ferrites with general formula $Co_xZn_{1-x}Fe_2O_4$ at (x = (0.5, 0.6, 0.7). the improvement of zinc has a significant influence on dielectric parameters and magnetic properties.

2. Experimental Method

2.1. Materials

All chemicals are of analytical mark. They are widely used as received, with no extra purification. Iron (III) nitrate ($Fe(NO_3)_3{\cdot}9H_2O$) – (SDH-USA), cobalt(II)- nitrate ($Co(NO_3)_2{\cdot}6H_2O$)-(Crist Purisimo Germany), Zinc nitrate ($Zn(NO_3)_2{\cdot}6H_2O$) - India, Citric Acid ($C_6H_8O_7{\cdot}H_2O$) - (Romil pure chemistry. UK), Deionized water and ammonia solution, was used to prepare the all ferrite samples.

2.2. Method of Preparation Ferrites

The sol-gel auto combustion method has been used to synthesize ferrite samples. A proper amount of metal nitrates Cobalt nitrate ($Co(NO_3)_2{\cdot}6H_2O$) or Zinc nitrate ($Zn(NO_3)_2{\cdot}6H_2O$) and citric acid was first dissolved in a minimum amount of deionized water. The molar ratio of cobalt and ferric nitrates ($Fe(NO_3)_3{\cdot}9H_2O$) was 1:2. The nitrates of citric acid ratio was 1:3. The mixed solution was stirred magnetically at room temperature and the pH of the solution was adjusted to 7 using ammonia solution. They were added in the form of drops with continuous mixing by magnetic stirrer. The additional water was removed by continue stirring heat at 60-80°C till a gel was obtained. The solution became brown color and the size of the solution became less and totally converted into a gel until all gels were completely burnt out at 220°C to form a fluffy loose structure (ash).

Table 1 shows examples of the raw materials and weight in (g). They were used to prepare $Co_{0.5}Zn_{0.5}Fe_2O_4$.

The ash material was ground well in a mortar and sintering at (400, 600, 800 and 1000°C) for 3 hrs. to get Cobalt ferrite ($CoFe_2O_4$) and Cobalt Zinc ferrite nanoparticles. Finally, the ash powder was divided into four groups and coded as indicated in Table 2:

Table 1. Raw materials used to prepare $Co_{0.5}Zn_{0.5}Fe_2O_4$.

Item No.	Materials	Weight (g)
1	$Co(NO_3)_2{\cdot}6H_2O$	4.36
2	$Zn(NO_3)_2{\cdot}6H_2O$	4.46
3	$Fe(NO_3)_3{\cdot}9H_2O$	24.24
4	(Citric Acid) -$C_6H_8O_7{\cdot}H_2O$	18.9

Table 2. Group samples divided for present research.

No.	Samples	Code
1	$CoFe_2O_4$	CF
2	$Co_{0.5}Zn_{0.5}Fe_2O_4$	CZF1
3	$Co_{0.6}Zn_{0.4}Fe_2O_4$	CZF2
4	$Co_{0.7}Zn_{03}Fe_2O_4$	CZF3

2.3. Instrument used for characterization

X-ray diffractometer (XRD) type (Shimadzu-6000-Japan) using Cu-Kα radiation (λ = 1.54060 Å). Fourier transform infrared (FTIR) spectroscopy type (Shimadzu-8400s - Japan) was used for the analysis of the chemical bond of sample, which XRD provided no information.

Morphology and particle size of the samples were also estimated by (SPM) subjecting them to scanning probe microscopic (Model: AA3000 Angstrom Advanced Inc., USA, AFM contact mode). Hysteresis loop parameters at room temperature were evaluated using a vibrating sample magnetometer (VSM), (Model: Lakeshore 7404 series, Ohio-USA). Dielectric permittivity of the sample was also measured using an Impedance Analyzer (HP 4294A, USA) in the frequency range 50 Hz-5 MHz. Furnace 1200°C type (THERM CONCEPT-Germany) for sintering samples at high temperatures.

Hotplate with magnetic stirrer Model (WiseStir-MSH-20A- was used to prepare chemical compositions of ferrite). Programmable Oven - 220°C type (Memmert GmbH-Achamber was used for heating or drying). pH meter (type HANNA- HI 2211-was used to measure the acidity and alkalinity of solution).

3. Results and Discussion

3.1. Structural and Phase Analysis

Figure 1 shows that X-ray diffraction (XRD) patterns of the spinel ferrite of cobalt ferrite CF and Cobalt-Zinc ferrites CZF1, CZF2, CZF3 obtained different temperatures. Peak patterns would be changed according to the composition. The absence of extra peaks might be due to the spinel phase of ferrite which indicated that all the compositions contained only single phase of spinel structure. The patterns indicated well-defined peaks of crystalline

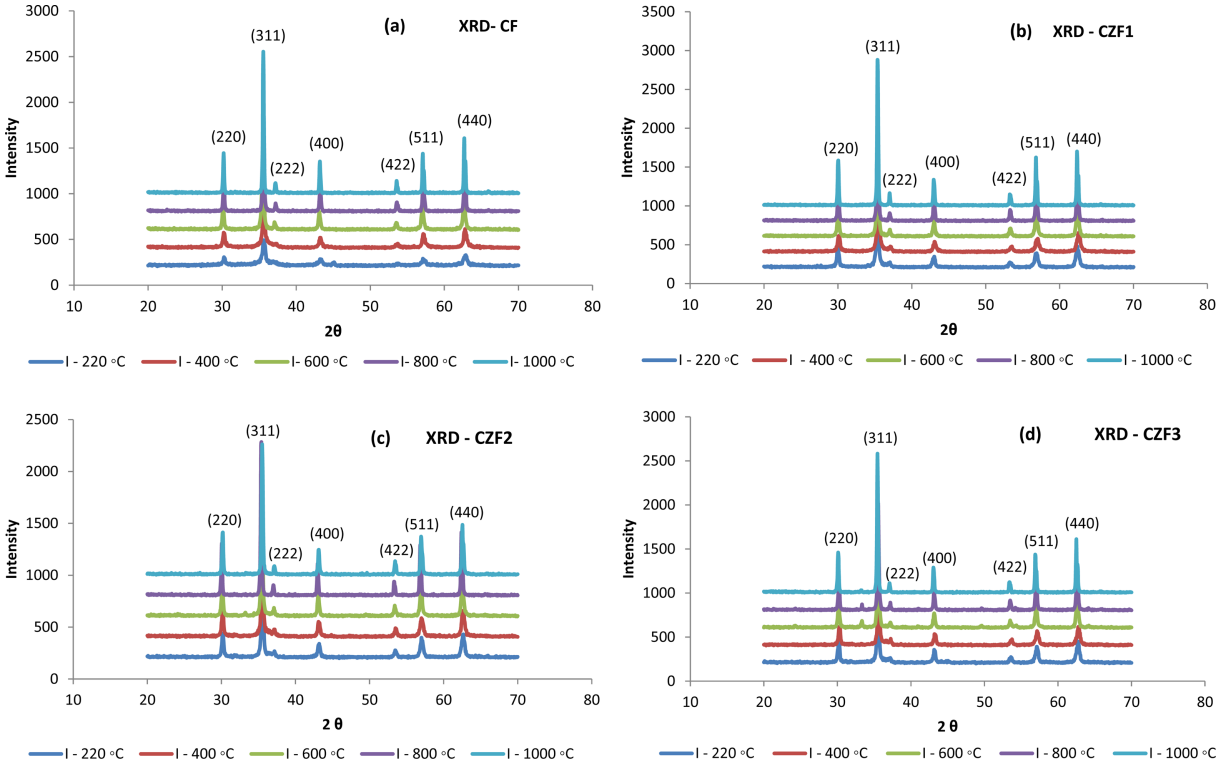

Fig. 1. (Color online) (a-d) Shows the XRD pattern of CF & CZF with different temperatures.

FCC structure. They confirmed spinel cubic phase formation. The peaks appeared at $2\theta = 30.14^o$, 35.49^o, 37.11^o, 43.12^o, 53.52^o, 57.03^o and 62.63^o, they matched to indicate (220), (311), (222), (400), (422), (511) and (440) respectively. All the peaks have good match with the standard pattern of bulk $CoFe_2O_4$ (JCPDS 22-1086). The zinc substitution process brought about different modifications in the structural properties such as lattice constant, unit cell volume, ionic radii, the distance between the magnetic ions and bond lengths on tetrahedral sites and octahedral sites of cubic spinel structure for the produced cobalt ferrite crystallites. The supermagnetic of Co-Zn ferrite increase with the concentration of zinc increases. And this result could be attributed to the higher ionic radius of zinc than that of cobalt species [18].

Crystallite size of nanoparticles was determined from the strongest peak (311) of XRD using the Scherrer formula:

$$D = 0.9\lambda/\beta\cos\theta \quad (1)$$

Where, λ is the wavelength of radiation used, β and θ is full width at half maximum (FWHM) and angle of strongest intensity peak, respectively. Table 3 is a calculation of strongest peak (311) crystallite size vs. temperature.

The average grain size has been found to increase the sintering temperature, while decreased with the increase of zinc content. Lattice constant "a" can be calculated from miller indices (h k l) using the relation:

$$a = d_{hkl}\sqrt{h^2 + k^2 + l^2} \quad (2)$$

Where (d) is the interplanar distance which is calculated from Bragg's law, ($n\lambda = 2d \sin\theta$, where n is an integer and λ is the x-ray wavelength).

The value of lattice constant (a) for CF, CZF1, CZF2, CZF3 ferrites represented in Table 4. The shortest distance between magnetic ions occupied at tetrahedral (A) and octahedral (B) lattice sites considering lattice constant, known as hopping length, can be calculated by using the following relation [19]:

$$L_A = a\sqrt{3}/4 \text{ and } L_B = a\sqrt{2}/4 \quad (3)$$

Table 3. Crystallite size (D) vs temperature at strongest peak (311).

Temp. °C	CF - D (nm)	CZF1 - D (nm)	CZF2 - D (nm)	CZF3 - D (nm)
220	18.48	21.64	25.35	26.55
400	25.31	22.88	27.49	27.22
600	28.55	28.05	30.08	26.26
800	41.18	34.78	49.39	42.76
1000	51.02	50.47	42.77	49.61

The calculated hopping and bond length values for tetrahedral (A) and octahedral (B) lattice sites for sample research were tabulated in Table 4. Theoretical X-ray density can be estimated from XRD pattern using the relation [19]:

$$N = \Sigma \frac{A}{N_A \times V} \quad (4)$$

Where (A) is the sum of atomic weights of all atoms in the unit cell, N_A is Avogadro's number and V is the volume of the unit cell. In spinel structure each primitive cell consists of eight molecules, so in our case the above relation can be rewritten as:

$$N = \Sigma \frac{8M}{N_A \times a^3} \quad (5)$$

Where M is the molecular weight of the nanoparticle and a^3 is volume of cubic unit cell. The calculated value of X-ray density of nanoparticles was found to be as given in Table 4. It is clearly seen from Table 4, the X-ray density of samples were used in this research increased linearly with increasing (Zn) concentration of $CoFe_2O_4$. This is due to the heavier weight of zinc atom compared with that of cobalt atom.

3.2. FTIR Characterization

The effects of the substitution of (Zn) in $CoFe_2O_4$, clearly appear via Fourier transform infrared spectroscopy FTIR. Two absorption bands ν_1 and ν_2 are observed in their spectra corresponding to the tetrahedral and octahedral clusterssites, which are signatures for spinel structure ofthe samples. These two structures confirm also the presence of M-O stretching band in ferrites [20].

The FTIR spectra at three different temperatures (220, 600, 1000°C) for the four samples (CF, CZF1, CZF2, CZF3) are shown in Fig. 2(a-d). The spectra value recorded in Table 5, the higher frequency band at 600°C, (ν_2)

Table 5. FTIR-Spectra absorption band at different temperature.

Sample	Sintering T °C	ν_1-cm^{-1}	ν_2-cm^{-1}
CF	220°C	399.26	567.07
CZF1		423.66	611.91
CZF2		405.79	620.74
CZF3		417.90	628.96
CF	600°C	414.45	633.62
CZF1		429.62	592.02
CZF2		404.70	581.38
CZF3		413.18	476.28
CF	1000°C	430.42	576.12
CZF1		407.122	1037.45
CZF2		420.82	596.85
CZF3		399.95	523.83

Table 4. Lattice parameter, crystallite size, X-ray density and hopping length of CF, CZF1, CZF2, CZF3 at different temperatures.

Sample	Sintering T °C	Lattice constant (a) - (Å)	Crystallite Sizes - D (nm)	X-Ray Density (g/cc)	L_A	L_B
CF	220°C	8.346	18.47	5.45	0.359	0.293
CZF1		8.411	21.64	5.31	0.364	0.297
CZF2		8.369	25.35	5.39	0.362	0.296
CFZ3		8.367	26.56	5.38	0.362	0.296
CF	400°C	8.351	25.31	5.35	0.362	0.295
CZF1		8.384	22.88	5.37	0.363	0.296
CZF2		8.372	27.49	5.37	0.362	0.295
CFZ3		8.347	27.22	5.42	0.361	0.295
CF	600°C	8.381	28.55	5.30	0.363	0.296
CZF1		8.406	28.05	5.33	0.364	0.297
CZF2		8.388	30.08	5.35	0.363	0.296
CFZ3		8.367	26.26	5.38	0.362	0.296
CF	800°C	8.358	41.18	5.35	0.362	0.295
CZF1		8.402	34.78	5.331	0.364	0.297
CZF2		8.403	49.40	5.317	0.364	0.297
CFZ3		8.367	42.76	5.38	0.362	0.296
CF	1000°C	8.364	51.02	5.33	0.362	0.296
CZF1		8.406	50.47	5.33	0.364	0.297
CZF2		8.374	42.78	5.37	0.362	0.296
CFZ3		8.386	49.61	5.34	0.363	0.296

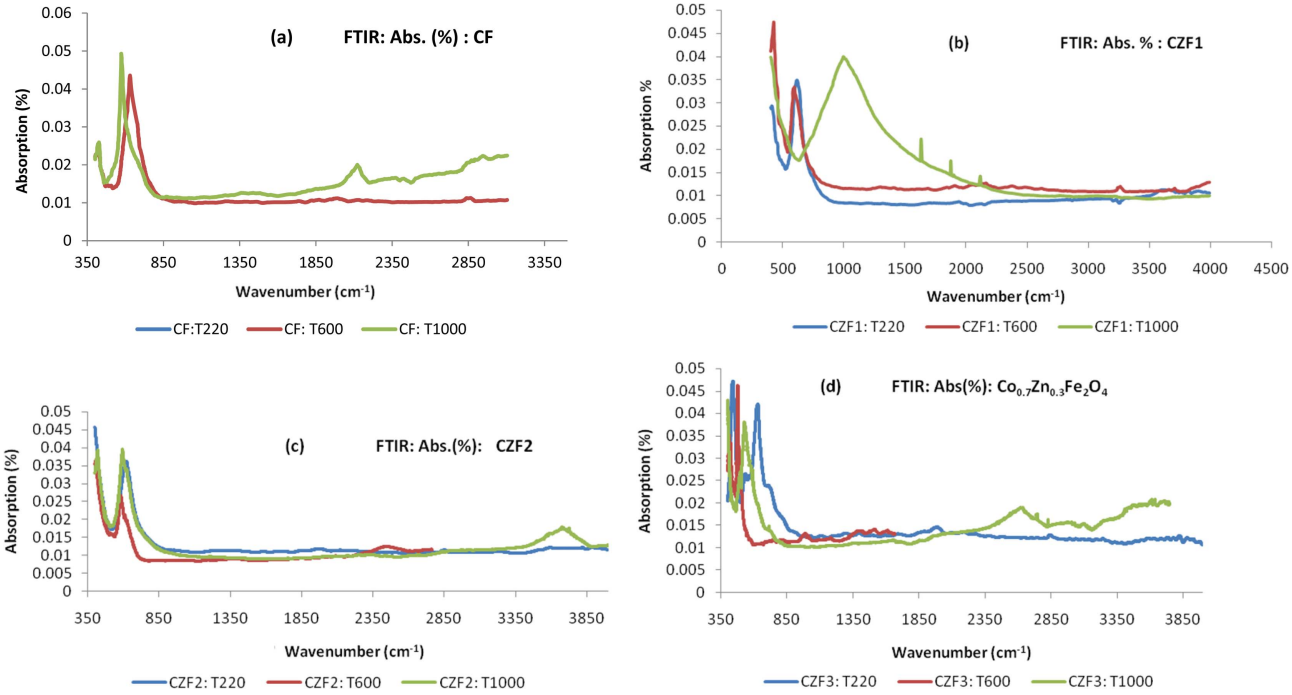

Fig. 2. (Color online) (a-d) FTIR-Spectra absorption bands at different temperatures.

was (633-476 cm^{-1}) and lower frequency band (ν_1) (414-413 cm^{-1}) was assigned to the tetrahedral and octahedral complexes [21]. This is may be due to that the normal form of vibration for tetrahedral cluster is higher than that of octahedral. It should be ascribed to the shorter bond length of tetrahedral cluster and longer bond length of octahedral cluster.

3.3. Atomic Force Microscopy (AFM)

Figure 3(a, b) showed two pictures of CF and CZF1 in 2D & 3D, which confirmed the rough nature of the samples with a good crystalline constructed by spherical grains with a narrow distribution of size. The particles size determined in Table 6 give a comparison result between the crystallite size calculated by XRD and AFM. The XRD is smaller than that obtained from AFM three times, because the AFM give the size of multiple crystalline as well as roughness, while XRD calculated the size of single crystal. This may be also happen because AFM gives the particles size with surroundings such as oxides [22].

Table 6. Comparison result between grain sizes determined by XRD and AFM as well as roughness.

Samples	XRD Crystallite size (nm)	AFM Crystallite size (nm)	Roughness (nm)
CF	28.55	76.18	0.955
CZF1	28.05	83.78	0.321
CZF2	30.08	81.17	0.616
CZF3	26.26	111.71	0.414

3.4. Magnetic Properties

Figure 4 shows the magnetization (M) as a function of applied magnetic field (H) for two samples CF & CZF1, sintered at 600°C. The characteristic of spinel ferrite such as coercivity (H_c), saturation magnetization (M_s), remanance magnetization (M_r) and squareness takes effect in decreases substance zinc in cobalt ferrite as seen in Table 7.

The field hysteresis loop shows a decreasing inclination in corecivity with Zn contents due to increased magnetic softness [22]. The decrease in these values results from the subsistence of spin deviation, which has been reported in several nanometer sized ferrites [23]. The low values of M_r/M_s ratio indicate a significant portion of superparamagnetic particles. M_r/M_s decreases from 1.0 to 0.00 indicating a portion of the particles in the closed state, [24, 25]. The application of a sufficiently large magnetic field and here was 12000 G (12 KOe). Oersted (Oe) is the unit of magnetic field strength in centimeter-gram-second (cgs) system (SI). It causes the spins come to an end to be aligned within a material and field, and the total magnetization decreases [26]. The shape of the hysteresis loop is especially of interest for magnetic recording applications,

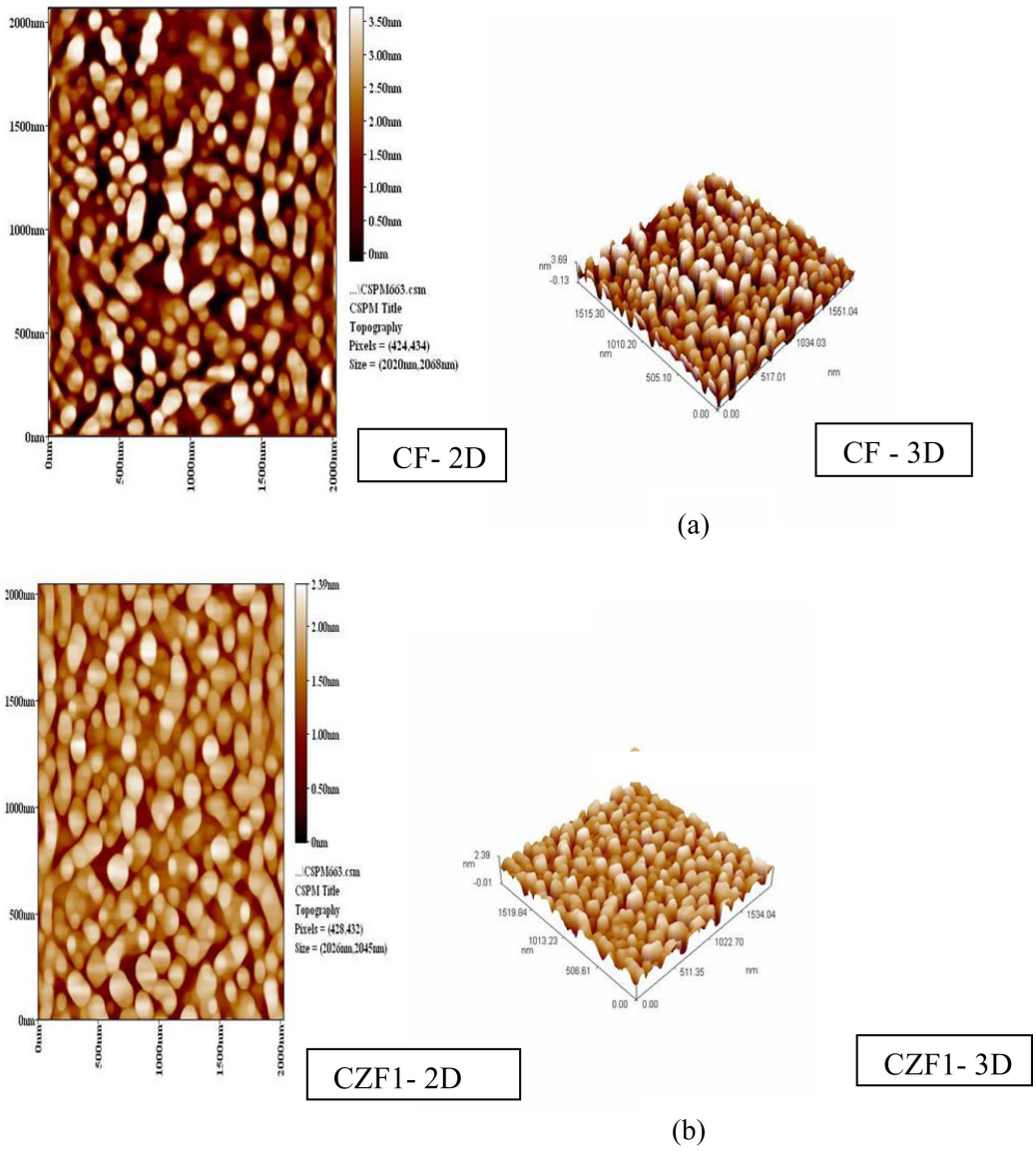

Fig. 3. (Color online) Picture of AFM in 2D & 3D: (a) - CF, (b) - (CZF1).

Table 7. Magnetic property of cobalt - Zinc ferrite.

Samples	Coercivity (H_c) G (Oe)	Saturation Magnetization (M_s) emu/g	Remanance Magnetization (M_r) emu/g	Remanance Ratio M_r/M_s (Squarenes)
CF	1292.7	91.604	49.970	0.54549
CZF1	95.413	29.700	4.8506	0.16332

which require a large remanent magnetization, moderate coercivity and (ideally) a square hysteresis loop [27].

3.5. Dielectric properties

Figure 5 showed that the supporting favor of the dielectric constant decreases with increased frequency, and it can be seen that the dispersion in (ε') is analogous to Maxwell-Wagner interfacial polarization [28, 29], and in agreement with Koop's phenomenological theory [30]. The polarization in ferrites is through a mechanism similar to the conduction process by electron exchange between Fe^{2+} and Fe^{3+}, the local displacement of electrons in the direction of the applied field occurs and these electrons determine the polarization. The polarization decreases by increasing the frequency and approaches to a constant value due to the electron exchange between Fe^{2+} and Fe^{3+}

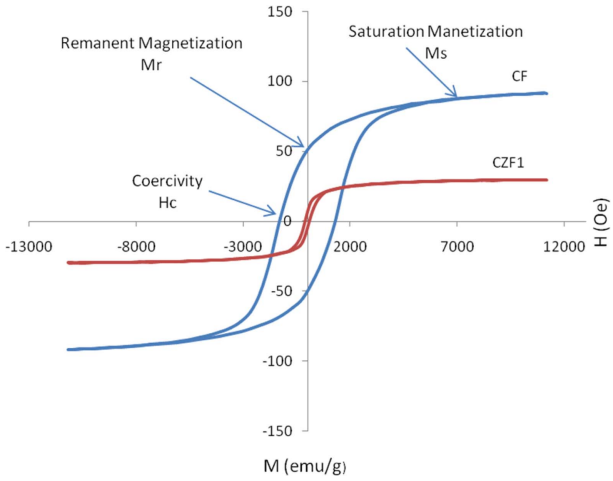

Fig. 4. (Color online) Hysteresis loop of CF & CZF1.

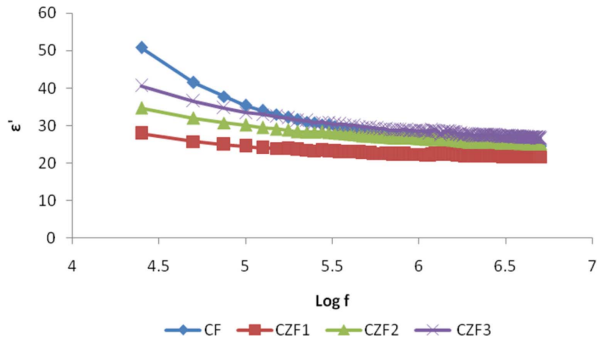

Fig. 5. (Color online) Real dielectric constant (ε') vs Log f.

cannot follow the alternating field [16]. There are two mechanisms responsible for the permittivity dispersion for polycrystalline ferrites at higher frequency; they are ion and electron polarization [31]. The oxygen ion vacancies produced during the synthesis may too contribute to dielectric permittivity which is majority at lower frequencies [32]. It can be seen that the sample shows the frequency-dependent phenomena, i.e., the dielectric constant decreases with increasing frequency. This is a normal behavior observed in most of the ferromagnetic materials, which may be due to the interfacial polarization [33, 34].

Figure 6 represents the dielectric loss factor (ε'') is an important part of the total core loss in ferrites [35]. The present ferrite nanoparticles with comparatively lower losses could be useful at frequencies higher than those of the individual ferrites [36]. The dielectric loss profiles are similar to those of dielectric constant.

Figure 7 shows the variation of tan δ at room temperature as a function of applied field frequency. It can be seen that a small irregular performance was observed for all the samples at different frequencies. According to Rezlescu model the relaxation peak may be due to the

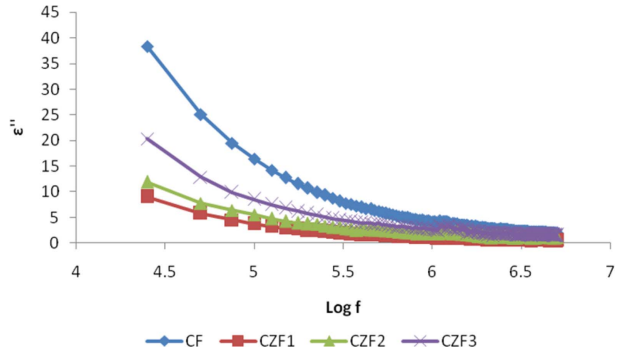

Fig. 6. (Color online) Imaginary dielectric constant (ε'') vs Log f.

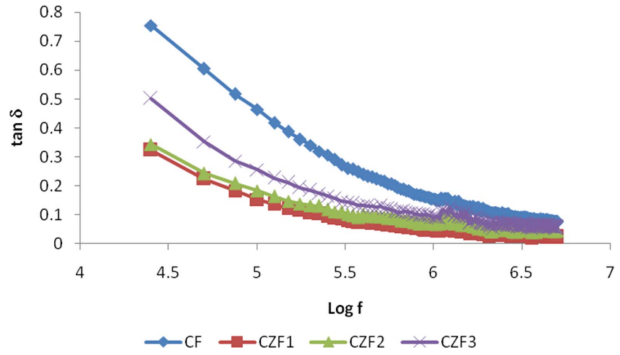

Fig. 7. (Color online) tan δ vs Log.

collective contribution of both p and n type of charge carriers [37]. The electronic exchange between $Fe^{2+} \Leftrightarrow Fe^{3+}$ and hole transfer between $Co^{2+} \Leftrightarrow Co^{3+}$ in octahedral sites are responsible for such behavior [10].

4. Conclusion

Sol-gel method has been employed to synthesize CF&CZF1, CZF2, CZF3 ferrite samples at nanometer scale. The spinel ferrites have been sintered at (220, 400, 600, 800 and 1000ºC) for three hours. The presence of Zinc (Zn) ions causes significant changes in the structural and magnetic properties of the CF as convert CZF1, CZF2, CZF3 ferrite. The X-ray diffraction characterized formation of single phase spinel structure and the grain size within nanosize. The average grain size has been found to increase with the sintering temperature, while it decreases with the increase of zinc content. As discovered by the observed results, the magnetic properties of the samples are mainly dominated by Zn^{2+} non magnetic ions replacing Co^{2+} ions as well as migration of Fe^{3+} ions from octahedral to tetrahedral sites. The field hysteresis loop shows a decreasing trend in saturation magnetization, remanent magnetization, coercivity and squarenes with Zn contents due to increased magnetic softness. All values

were sufficiently low to confirm that the ferrite was a soft ferrite. Experimental data shows all investigational data reveals that the zinc substitution performing an explanation responsibility to change its structural and magnetic properties significantly.

References

[1] S. Nasrin, S. M. Hoque, F.-U.-Z Chowdhury and M. M. Hossen, IOSR-JAP. **6**, 58 (2014).
[2] D. S. Mathew and R. S. Juang, J. Chem. Eng. **129**, 51 (2007).
[3] L. R. Gonsalves, L. R. Gonsalves, S. C. Mojumdar, and V. M. S. Verenkar, J. Therm. Anal. Calorim. **104**, 869 (2011).
[4] M. Sertkol, Y. Köseoğlu, A. Baykal, H. Kavas, and A. C. Bas-aran, J. Magn. Magn. Mater. **321**, 157 (2009).
[5] F. Gözüak, Y. Köseoğlua, A. Baykal, and H. Kavas, J. Magn. Magn. Mater. **321**, 2170 (2009).
[6] H. Y. He, J. Mater. Sci.: Mater Electron **23**, 995 (2012).
[7] L. Victoria, C. Calero-Ddel, and Carlos Rinaldi, J. Magn. Magn. Mater. **314**, 60 (2007).
[8] R. Arulmurugan, B. Jeyadevanb, G. Vaidyanathana, and S. Sendhilnathan, J. Magn. Magn. Mater. **288**, 470 (2005).
[9] Y. Köseoğlu, A. Baykal, F. Gözüak, and H. Kavas, Polyhedron **28**, 2887 (2009).
[10] I. H. Gul and A. Maqsood, J. Alloys Compd. **227**, 465 (2008).
[11] M. M. Ismail and N. A. Jaber, Surf. Rev. Lett. (2017) https://doi.org/10.1142/S0218625X18500762
[12] G. De, G. Mattei, P. Mazzoldi, C. Sada, G. Battaglin, and A. Quaranta|, Chem. Mater. **12**, 2157 (2000).
[13] S. B. Waje, M. Hashim, W. Daud, W. Yusoff, and Z. Abbas, J. Magn. Magn. Mater. **322**, 686 (2010).
[14] J. López, L. F. González-Bahamón, J. Prado, J. C. Caicedo, G. Zambrano, M. E. Gómez, J. Esteve, and P. Prieto, J. Magn. Magn. Mater. **324**, 394 (2012).
[15] A. Hassadee, T. Jutarosaga, and W. Onreabroy, Procedia Eng. **32**, 597 (2012).
[16] I. H. Gul, A. Z. Abbasi, F. Amin, M. Anis-ur-Rehman, and A. Maqsood, J. Magn. Magn. Mater. **311**, 494 (2007).
[17] M. Veverka, Z. Jirák, O. Kaman, K. Knížek, M. Maryško, E. Pollert, K. Závěta, A. Lančok, M. Dlouhá, and S. Vratislav, Nanotechnology **22**, 345701 (2011).
[18] V. G. Patil, Sagar E. Shirsath, S. D. More, S. J. Shukla, and K. M. Jadhav, J. Alloys Compd. **488**, 199 (2009).
[19] Z. Karimi, Y. Mohammadifa, H. Shokrollahi, Sh. KhamenehAsl, Gh. Yousefi, and L. Karimi, J. Magn. Magn. Mater. **361**, 150 (2014).
[20] A. Pradeep and G. Chandrasekaran, Mater. Letter. **60**, 371 (2006).
[21] S. S. Patil, V. C. Mahajan, M. G. Patiland, and S. D. Lotke, J. Mater. Sci. **34**, 6063 (1999).
[22] G. Dixit, J. P. Singh, R. C. Srivastava, and A. Gupta, Indian J. Pure and Applied Physics **48**, 287 (2010).
[23] S. Nasrin, S. Manjura Hoque, F. U. Z. Chowdhury, and M. MoazzamHossen, J. Appl. Phys. (IOSR-JAP), **6**, 58 (2014).
[24] A. E. Berkowitz and W. J. Schuele, J. Appl. Phys. **39**, 1261 (1968).
[25] R. T. Denton and E. G. Spencer, J. Appl. Phys. **33**, 1300 (1962).
[26] H. K. Jun, Tae Jin Lee, Si Ok Ryu, and Jae Chang Kim, Energy Fuels **18**, 41 (2004).
[27] D. S. Mathew and R. S. Juang, Chem. Eng. J. **129**, 51 (2007).
[28] D. L. Leslie-Pelecky and R. D. Rieke, Chem. Mater. **8**, 1770 (1996).
[29] A. M. M. Farea, Shalendra Kumar, and Khalid Mujasam-Batoo, J. Alloys Compd. **464**, 361 (2008).
[30] R. D. McMichael, R. D. Shull, L. J. Swartzendruberand, and L. H. Bennett, J. Magn. Magn. Mater. **111**, 29 (1992).
[31] C. G. Koops, Phys. Rev. **83**, 121 (1951).
[32] G. C. Psarras, Composites: Part A **37**, 1545 (2006).
[33] N. Ponpandian and A. Narayanasamy, J. Appl. Phys. **92**, 2770 (2002).
[34] S. Sindhu, S. Sindhu, M. R. Anantharaman, B. P. Thampi, K. A. Malini, and P. Kurian, Bull. Mater. Sci. **25**, 599 (2002).
[35] E. M. Mohammed, K. A. Malini, Philip Kurian, and M. R. Anantharaman, Mater. Res. Bull. **37**, 753 (2002).
[36] J. Zhu, K. J. Tseng, and C. F. Foo, IEEE Trans. Magn. **36**, 3408 (2000).
[37] A. S. Hudson, Marconi Rev. **37**, 43 (1968).
[38] N. Rezlesecu and E. Rezlescu, Phys. Stat. Sol (a) **23**, 575 (1974).